SAND2017-8944C

SOLUTION MINING RESEARCH INSTITUTE
www.solutionmining.org

105 Apple Valley Circle
Clarks Summit, PA 18411, USA

Telephone: +1 570-585-8092

Technical Conference Paper

Salt Fall Detection in Oil Storage Caverns

Pierre Bérest, LMS, Ecole Polytechnique, France
Benoît Brouard & Vassily Zakharov, Brouard Consulting, France
Dean Checkai, Fluor Federal Petroleum Operations, USA
David Hart, Sandia National Laboratories, USA

SMRI Fall 2017 Technical Conference
25 - 26 September 2017
Münster, Germany

Solution Mining Research Institute Fall 2017 Technical Conference
Münster, Germany, 25 - 26 September 2017

Salt Fall Detection in Oil Storage Caverns

Pierre Bérest[1], Benoît Brouard[2], Dean Checkaï[3],
Hakim Gharbi[1], David Hart[4], Vassily Zakharov[2]

[1] Ecole Polytechnique, Palaiseau, France

[2] Brouard Consulting, Paris, France

[3] Fluor Federal Petroleum Operations, LLC, USA

[4] Sandia National Laboratories, Albuquerque, NM, USA

Abstract

In an oil storage cavern, salt block fall generates pressure waves. These waves can be recorded at the brine string wellhead. An example of this was provided in a paper presented during the Albuquerque SMRI Meeting by Hart et al. (2017). In the present paper, it is suggested that these pressure changes originate from gravity waves such that the brine-oil interface swings in the cavern. These events are easier to record when the brine string shoe is not too deep below the oil/brine interface (h_b on Figure 1) and when the offset between the brine string shoe and the cavern axis of symmetry is large enough (r_s on Figure 1). Some information on block size can be inferred from the analysis of pressure waves.

Key words: Caverns for Oil storage, Cavern Testing, Waves in Salt Caverns, SPR, Big Hill.

Introduction

Salt falls are relatively frequent in salt caverns (Cole, 2002; Munson et al., 2004; Rokahr et al., 2007; Crotogino et al., 2001; Baar, 1977; Renoux et al., 2013). In some cases, strings are broken during the salt fall. However, in many cases, they remain unobserved until there are revealed by a sonar survey or a gamma ray, performed several months or years after the fall, which detect shape change or bottom heave

In natural gas caverns, sluffing and creep closure occur. The former generates no cavern volume change; however, both contribute to the raise of the gas-brine interface. Special methods allow discriminating between these two possible causes (Cole, 2002).

In oil storage caverns, cavern pressure is higher than in gas cavern and creep closure is slower. Several techniques can be used to detect salt falls in real time. The simplest consists of recording accurately brine pressure (P_b) and oil pressure (P_o) at the wellhead. When γ_o and γ_b are oil and brine volumetric weight, respectively, and *h* is the oil/brine interface depth:

$$P_o - P_b = (\gamma_b - \gamma_o) h \quad (1)$$

The exact values of γ_o and γ_b cannot be not *perfectly* known ($\gamma_b = 0.012$ MPa/m $= 0.52$ psi/ft and $\gamma_o = 0.0085$ MPa/m $= 0.37$ psi/ft are typical), making any assessment of interface depth (h) uncertain. However, when comparing two *successive* positions of the interface, uncertainties are much smaller, $\delta(P_o - P_b) = (\gamma_b - \gamma_o)\delta h$, as volumetric weights remain constant. Consider for instance a cylindrical cavern whose diameter is 200 ft (60 m); its cross-sectional area is *S* = 31,000 ft^2 = 2800 m^2. A 1000 m^3-block falling from the upper part of the cavern generates an interface rise by $\delta h = 0.35$ m, or 1 ft, and a differential pressure change $\delta(P_o - P_b) = (0.52 - 0.37) \times 1 = 0.15$ psi ≈ 11 mbar,a value which is small but can easily be detected when accurate pressure sensors are used.

Renoux et al. (2013) describe continuous digital microseismic monitoring performed since 1992 at Geosel-Manosque in France where a 27-cavern oil storage is operated; 10,000 induced microseismic events with magnitude lower than 0.3 have been located within the storage perimeter. Some of them originate in block fall events. Event location is of prime importance in this context as it allows a better understanding of cavern mechanical behavior.

In this paper, it is suggested that wellhead pressure evolution, when properly recorded at ground level, provides useful information on salt block falls.

Waves in a salt cavern

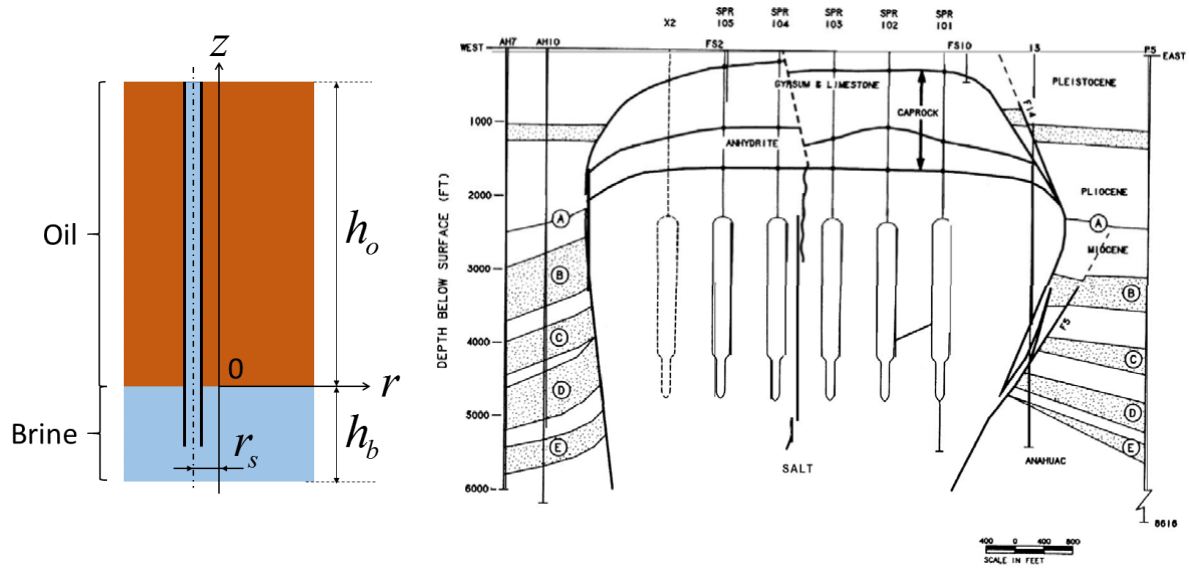

Figure 1 - The « box » (Park et al., 2005).

Many kinds of waves can be generated by pressure changes in a salt cavern (Berest et al., 1999). Here, we are mainly interested in stationary waves (in the liquid body, oscillations phase is the same at any point) that develop some time after the transient waves which result from the initial pressure change vanish. They include:

- Quarter-waves in strings and annular spaces. Their period is $T = 4H/c$ where H is the distance from the wellhead to the tube (or annular space) shoe and c the velocity of sound in the string. Sound velocity in brine is $c = 1800$ m/s (5900 ft/s); however sound velocity in a brine-filled string is slower, as the steel string is somewhat compressible too. When string thickness and stiffness are known, sound velocity in the string can easily be computed (or measured). In a brine-filled string, it is $c = 3900$ ft/s (1200 m/s), typically, and when the brine string is

$H = 3900$ ft - (1200 m-) long, quarter-waves period in the brine string is $T = 4$ seconds. In an oil-filled annulus, velocity of sound is c' = 1800 ft/s (600 m/s), typically; when this annulus is 2200-ft long (660 m), quarter-waves period in this annulus is $T = 4.4$ seconds.

- Resonator's waves. These waves can be observed when the upper part of a string or an annulus is partially filled with gas (for instance, during an MIT). Their period depends on gas column height.

- Interface waves. They can be observed in a cavern containing an interface between two non-miscible fluids (e.g., oil and brine). Equilibrium demands that this interface be horizontal. When, following a perturbation, interface departs from its horizontal equilibrium position, gravity forces tend to restore equilibrium. In sharp contrast with the waves described above, these waves do not result from fluids compressibility. Examples of such waves were described by Hart et al., 2017, who presented pressure records performed in BH112B (a brine well of a storage cavern at the Big Hill SPR site) following a salt fall (Figure 2):

  "*The waveform from this particular salt fall event shows a maximum amplitude of ~80 PSI (0.55 MPa), a period of ten to twenty seconds, and evidence of two distinct underlying frequencies. The event lasts a total of ten minutes before decaying to within the noise limits of the compression algorithm*." p. 14.

  In the following a tentative explanation of this phenomenon is proposed.

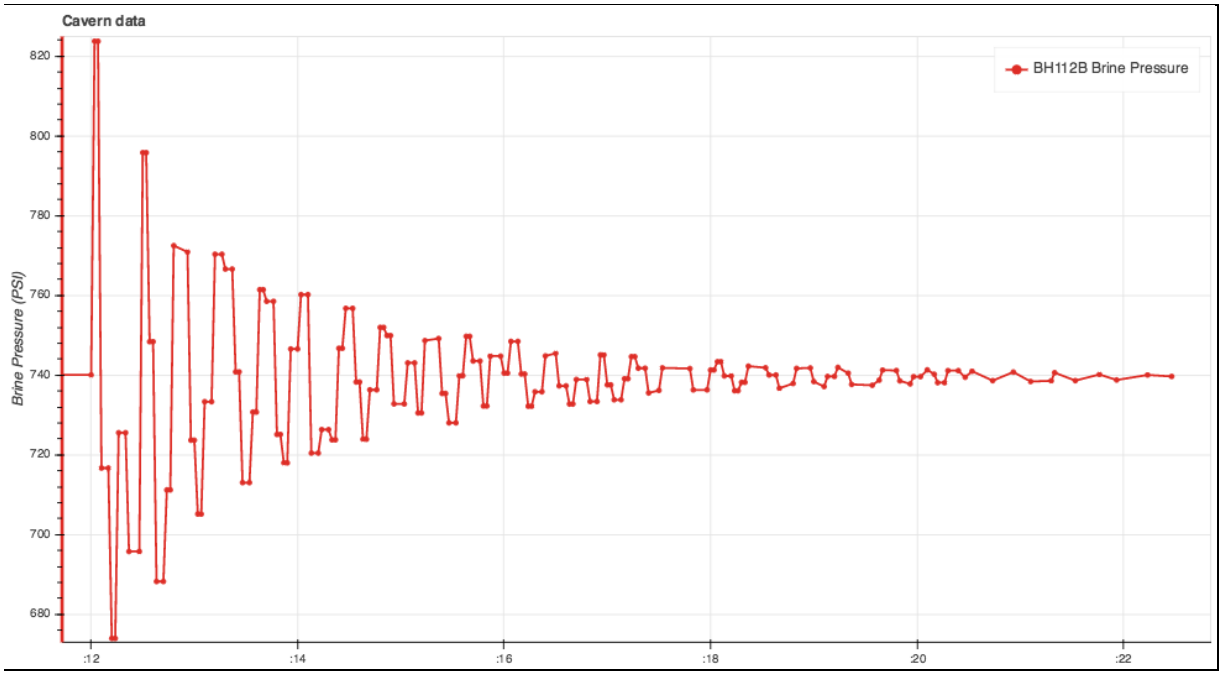

Figure 2 - Salt fall event pressure signature at the wellhead. Time scale is in minutes since 5:00 UTC (from Hart et al., 2017).

Gravity Waves

A simple mathematical description of the gravity waves can be reached when considering a closed cylindrical « box » (see Figure 1). To some extent, such a box mimics the elongated caverns of the Big Hill SPR site. The box contains a heavy fluid (brine) and a light fluid (oil). At equilibrium, the interface

coincides with the horizontal line $z=0$. Cavern bottom and cavern roof depth are $z=-h_b$ and $z=h_o$, respectively. Both fluids are non-viscous (the role of viscosity will be discussed later) and the momentum equation (Newton's equation) writes:

$$\rho\frac{d\underline{v}}{dt}=-grad\ p+\underline{g}\varrho \tag{2}$$

Fluids compressibility is neglected: fluid density is $\text{constant},\ \gamma=\rho g=\text{constant}$ and $\text{div}\ v=0;\ g$ is gravity acceleration. In the acceleration term of the momentum equation, only the linear term is considered: $dv/dt\approx\partial v/\partial t$. When only stationary waves are considered, it can be inferred that there exist two harmonic ($\Delta\psi=0$) functions, ψ_o and ψ_b such that $\underline{v}_o=\cos\omega t\ grad\ \underline{\psi}_o(r,\theta,z)$ and $\underline{v}_b=\cos\omega t\ \text{grad}\ \underline{\psi}_b(r,\theta,z)$, $p_o=-\gamma_o z-\frac{\gamma_o}{g}\frac{\partial\psi_o}{\partial t}$ and $p_b=-\gamma_b z-\frac{\gamma_b}{g}\frac{\partial\psi_b}{\partial t}$

Eigen modes

Solutions of $\Delta\psi=0$ satisfying the boundary conditions (fluid rate vanishes to zero at cavern walls, roof and bottom; at the brine-oil interface, oil rate and brine rate must be equal) can be written as a series of functions such that:

$$\begin{cases}\psi_o(r,\theta,z)=\sum_{n,i}\psi_o^{n,i}=\sum_{n,i}C_{n,i}^o\cos(n\theta)\ J_n\left(\alpha_{n,i}\frac{r}{R}\right)\text{ch}\left(\alpha_{n,i}\frac{z-h_o}{R}\right)\\ \psi_b(r,\theta,z)=\sum_{n,i}\psi_b^{n,i}=\sum_{n,i}C_{n,i}^b\cos(n\theta)\ J_n\left(\alpha_{n,i}\frac{r}{R}\right)\text{ch}\left(\alpha_{n,i}\frac{z+h_b}{R}\right)\end{cases} \tag{3}$$

Where $J_n(\alpha)$ is the n^{th} Bessel function of the first kind, $\alpha_{n,i}$ is the i^{th} root of $dJ_n(\alpha)/d\alpha=0$. In addition, pressure must be continuous through the oil-brine interface, leading to:

$$\omega_{n,i}^2=\frac{(\gamma_b-\gamma_o)g}{\alpha_{n,i}R\left[\gamma_b\coth\left(\alpha_{n,i}h_b/R\right)+\gamma_o\coth\left(\alpha_{n,i}h_o/R\right)\right]} \tag{4}$$

To each of these eigen values or $\omega_{n,i}$ is associated an eigen mode $\psi^{n,i}$, labelled (n,i). To each of these eigen modes is associated a shape of the maximum vertical displacement of the interface. The shape of the interface displacement for the four eigen modes whose periods ($T_{n,i}=2\pi/\omega_{n,i}$) are longest are represented schematically on Figure 3. For each of these eigen modes, one or several nodal lines can be defined (there is no interface displacement along a nodal line).

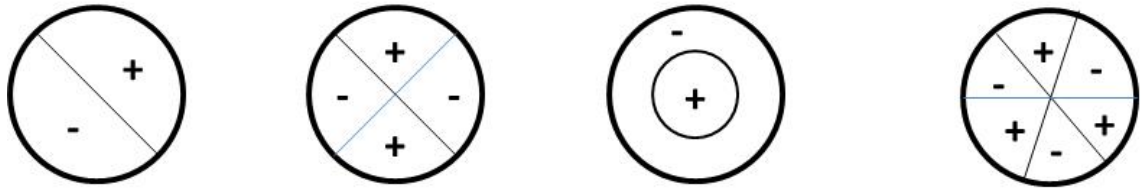

Figure 3 - First four eigen modes.

In principle, the double infinity of coefficients $C_{n,i}^o$ and $C_{n,i}^b$ can be computed when initial conditions are known. However, describing how the block drops down, hit the brine-oil interface and breaks when reaching the bottom of the cavern is out of reach. In fact, oil and brine are viscous and dampening

occurs. After some time, the eigen modes whose periods are shortest vanish as they are associated with high-frequency oscillations: dampening is faster when period is shorter. At the very beginning, the 2-3 first modes can be observed. After some time, from a practical point of view, only the first mode (1,1) is active. Its shape is provided on Figure 4 (This shape can be observed when rocking a water-filled plate).

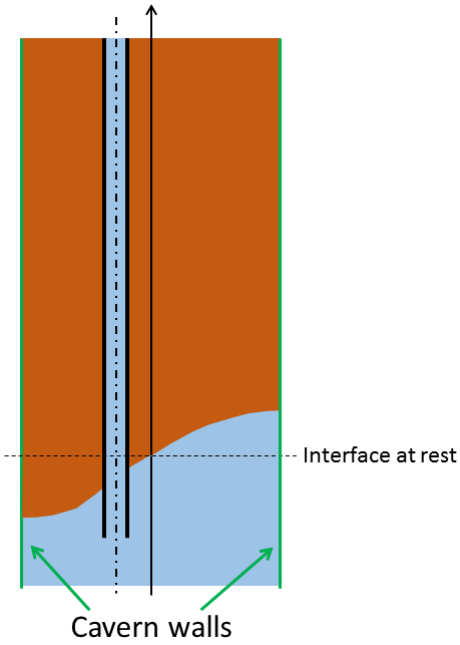

Figure 4 - First eigen mode (1,1), vertical cross section of the cavern.

Period of the first eigen-mode

In many cases, cavern radius is smaller than brine or oil height, $\alpha_{n,i} h_b / R$ or $\alpha_{n,i} h_o / R$ are much larger than 1 and

$$T_{n,i} \approx 2\pi \sqrt{\frac{(\gamma_b + \gamma_o) R}{(\gamma_b - \gamma_o) g \alpha_{n,i}}} \tag{5}$$

When $R = 33$ m (110 ft), the two first periods are $T_{1,1} = 20.6$ s and $T_{0,2} = 14$ s. On Figure 2, it is clear that, in the BH112B cavern, one minute after the block fall, pressure oscillations period is 20 seconds. However, immediately after the block fall, pressure changes are a combination of several modes – quarter waves in the wellbore may also play a role. Pressure sampling rate is not fast enough for an identification of all these modes.

Wave detection

When the first eigen mode (1,1) is considered, pressure changes in the brine body write:

$$\delta p_b = -\gamma_b \frac{\partial \psi_b}{\partial t} = -\gamma_b C \omega_{1,1} \sin(\omega_{1,1} t)\, sh\left(\frac{\alpha_{1,1} h_o}{R}\right) J_1\left(\alpha_{1,1} \frac{r}{R}\right) \cos(\theta)\, ch\left[\frac{\alpha_{1,1}(z + h_b)}{R}\right] \tag{6}$$

Where C (in meter) is a constant, $0 < r < R$, $-h_b < z < 0$, the nodal line is $\theta = \pi/2$, $\alpha_{11} \approx 1.8412$. Pressure changes are maximum at interface depth ($z = 0$) at cavern wall ($r = R$) on the diameter perpendicular to the nodal line ($\theta = \pi/2$); they are proportional to C:

$$\delta p_b^{\max} = \gamma_b C \omega_{1,1} sh\left(\frac{\alpha_{1,1} h_o}{R}\right) J_1(\alpha_{1,1})\, ch\left(\frac{\alpha_{1,1} h_b}{R}\right) \tag{7}$$

And:

$$\delta p_b = -\Delta p_b^{\max} \sin\left(\omega_{1,1} t\right) \cos\left(\theta\right) \frac{J_1\left(\alpha_{1,1} \frac{r}{R}\right)}{J_1\left(\alpha_{1,1}\right)} \frac{ch\left[\frac{\alpha_{1,1}\left(z+h_b\right)}{R}\right]}{ch\left(\frac{\alpha_{1,1} h_b}{R}\right)} \tag{8}$$

Pressure changes are measured at the wellhead of the brine string; they reflect pressure changes at the end of tubing (EOT) depth. In other words, pressure changes are larger (hence, easier to record) when end of tubing is closer from the cavern wall, closer from the brine-oil interface and farther from the nodal line. The pressure recording method is extremely cost effective; its main weakness lay in the fact that the end of tubing must be located conveniently.

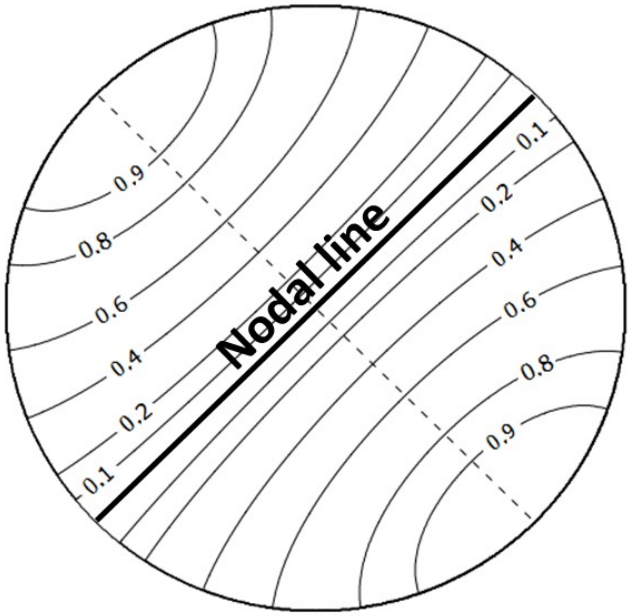

Figure 5. Relative brine pressure changes ($\delta p_b/\Delta p_b^{max)}$ at interface depth following a salt fall

Pressure changes and energy

When a salt block whose mass is M (kg) falls by h (m) to the bottom of the cavern, a Mgh potential energy is provided to the fluid-filled cavern. A part of this energy is converted into kinetic energy as the interface rolls up and down in the cavern; another part is lost because of viscous effects. After some time, the kinetic energy contained in the eigen modes whose period is shortest has dissipated and only the first eigen mode is observed. For this reason, it is interesting to compute the relation between the kinetic energy and the amplitude of the pressure changes when the first mode (1,1) is considered: recording pressure changes give an idea of the kinetic energy involved. However, it must be kept in

mind that this computed kinetic energy is only a part of the total energy Mgh that was provided to the system by the block fall.

When $\bar{K}_{1,1}$ is the oil and brine kinetic energy averaged during a period of the first mode, this relation is:

$$\frac{\bar{K}_{1,1}}{P^2_{\max 1,1}} = \frac{\pi}{16}\left(\alpha^2_{1,1} - 1\right)\frac{\left(\gamma_b - \gamma_o\right)Rg^2}{\omega^4_{1,1}\gamma^2_b \coth\left(\frac{\alpha_{1,1}h_b}{R}\right)} \tag{9}$$

Conclusion

Following salt falls, pressure waves are observed in oil storage caverns. They are generated by oil-brine interface oscillations. After some time, these oscillations become relatively simple as the interface rolls up and down in the cavern around a line (nodal line) which experiences no displacement. These oscillations can be measured at the wellhead. The observed signal strongly depends upon the location of the end of the brine tubing below the oil-brine interface. However the size of the salt block can be assessed, especially when the cavern experiences relatively frequent falls.

References

Baar C.A. (1977) - *Applied salt-rock mechanics*. Vol. I. Developments in Geotechnical Engineering. 16-A. Amsterdam: Elsevier Science.

Bérest P., Bergues J., Brouard B. (1999). *Review of static and dynamic compressibility issues relating to deep underground salt caverns*. Int. J. Rock Mech. Min. Sci., 36, 1031-1049.

Checkai D., Osborne G., Eldredge L, Lord D. (2014) *Pressure Trending Analysis to Support Cavern Integrity Monitoring at the U.S Strategic Petroleum Reserve*. SMRI Spring Meeting, San Antonio, Texas.

Cole R. (2002) - *The Long-Term Effects of High Pressure Natural Gas Storage on Salt Caverns*. SMRI Spring Meeting, Banff, Canada, 75-97.

Crotogino F., Mohmeyer K.U, Scharf R. (2001) - *Huntorf CAES: More than 20 Years of Successful Operation*. SMRI Spring Meeting, Orlando, Florida, 351-362.

Hart D., Bettin G., Bellevue B. (2017). *Pressure Trend Analyses for Geophysical and Integrity Investigations*. SMRI Spring Meeting, Albuquerque, New Mexico.

Renoux P., Fortier E., Maisons C. (2013) Microseismicity induced within Hydrocarbon Storage in Salt Caverns, Manosque, France. Hazard review and event re-location in a 3D velocity model. SMRI Fall Meeting, Avignon, France.

Munson, DE., Ehgartner, B., Bauer, S., Rautman, C., Myers, R. (2004). *Analysis of a salt fall in Big Hill Cavern 103, and a preliminary concept of salt dome structure*. SMRI Spring Meeting, Wichita, KS. 57-72.

Park B.Y., Ehgartner BL, Lee MY, Sobolik SR. (July 2005). *Three-Dimensional simulation for Big Hill strategic Petroleum Reserve (SPR)*. Sandia Report, SAND 2005-3216.

Rokahr R., Staudtmeister K., Zander- Schiebenhöfer D., Johansen J.I. (2007) - *In-situ Test with a Gas Storage Cavern as a Basis for Optimization*. SMRI Spring Meeting, Basel, Switzerland, 84-97.

Disclaimers

Sandia National Laboratories is a multimission laboratory managed and operated by National Technology and Engineering Solutions of Sandia LLC, a wholly owned subsidiary of Honeywell International Inc. for the U.S. Department of Energy's National Nuclear Security Administration under contract DE-NA0003525.